J Mater Sci: Mater Electron (2014) 25:4170–4178
DOI 10.1007/s10854-014-2145-2

# Phase transformation and fracture behavior of Cu/In/Cu joints formed by solid–liquid interdiffusion bonding

**Yanhong Tian · Chunjin Hang · Xin Zhao · Baolei Liu · Ning Wang · Chunqing Wang**

Received: 21 May 2014 / Accepted: 1 July 2014 / Published online: 9 July 2014


**Abstract** In this paper, microstructure evolution and phase transformation of Cu–In intermetallic compounds in Cu/In/Cu joints formed by solid–liquid interdiffusion bonding at 260 and 360 °C were investigated respectively. The shearing properties and fracture behaviors of the Cu/In/Cu joints formed under different bonding conditions were also studied. For Cu/In/Cu joints bonded at 260 °C, $Cu_{11}In_9$ phase firstly generated and then $Cu_2In$ phase formed between $Cu_{11}In_9$ layer and Cu substrate. For Cu/In/Cu joints bonded at 360 °C, $Cu_2In$ phase firstly formed and then parts of $Cu_2In$ grains transformed to $Cu_7In_3$ phase, and this transition from incomplete to complete coverage of $Cu_2In/Cu_2In$ grain boundaries by $Cu_7In_3$ phases was observed with the bonding time increasing. The shear test results show that $Cu_2In$ was high-quality phase which could improve the mechanical properties of Cu/In/Cu joints. After shear test, the fractures in Cu/In/Cu joints bonded at 260 °C were found at $Cu_{11}In_9$ layers and the fracture mode was cleavage fracture. In the case of the joints bonded at 360 °C, the intergranular fractures were found at the interface between $Cu_2In$ layer and $Cu_7In_3$ layer while the cleavage fractures were found at $Cu_7In_3$ layer.

## 1 Introduction

As the interconnection density continues to increase, 3D chip packaging technology which makes full use of space becomes greatly promising [1, 2]. Under this trend, solid–liquid interdiffusion (SLID) bonding method becomes a research hotspot with its unique advantages for interconnections [3, 4]. Through this method, low-temperature bonding process can be achieved by depositing high-melting-point metal and low-melting-point solder at bonding areas. After bonding, the joint would only contain high-melting-point intermetallic compounds and hence it can withstand high temperature during the subsequent reflowing process, which can reduce the risk of thermal mismatch problems [5–8].

Compared to the extensive studied Cu–Sn interconnections, the Cu–In interconnection exhibits better bonding properties as the required bonding temperature of Cu–In interconnections is lower than that of Cu–Sn interconnections [9–13]. Currently, the research activities of Cu–In system mainly focus on Cu–In intermetallic compounds theoretical analysis and their growth kinetics [14–17]. However, there is a lack of systematic study on microstructure evolution of Cu/In/Cu joints under different bonding conditions. Mechanical properties of Cu/In/Cu joints were also rarely reported.

Lee et al. [18] have studied the mechanical performance of Cu–Sn interconnections and found that the fracture mode of Cu–Sn joints was distinctively brittle fracture. It was also found that larger bonding pressure could improve the shear strength of Cu–Sn joints. In addition, the shear strength of Cu–Sn joints could be enhanced with higher bonding temperature. They also found that the fracture mode was brittle fracture and no significant plastic deformation was found in the stress–strain curves. It was also found that shear strengths were improved as bonding temperature increased. Lee et al. [19] have studied low-temperature bonding properties of Ag–In joints. The Ag–In joints consisting of single-phase $Ag_2In$ were obtained through the bonding process at 180 °C for 40 min and the annealing process for 24 h at 120 °C. Bernhard et al. [5]

Y. Tian (✉) · C. Hang · X. Zhao · B. Liu · N. Wang · C. Wang
State Key Laboratory of Advanced Welding and Joining, Harbin Institute of Technology, Harbin 150001, China
e-mail: tianyh@hit.edu.cn

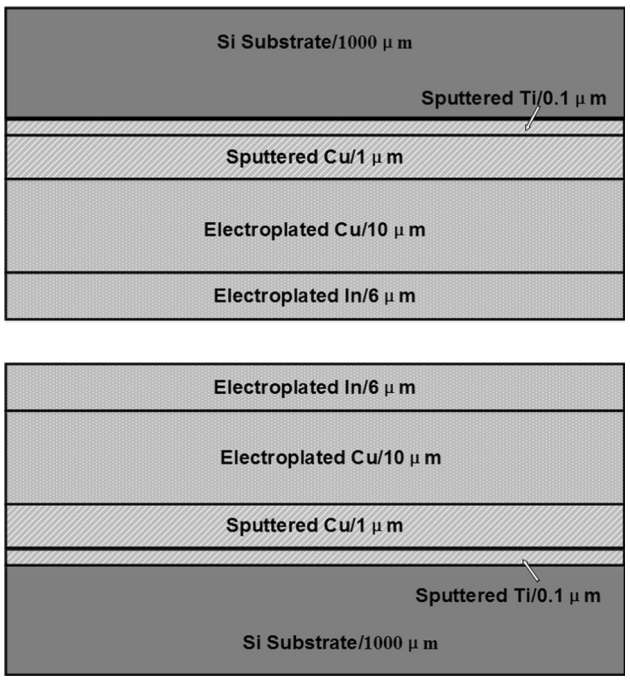


**Fig. 1** The schematic diagram of Cu/In/Cu joints

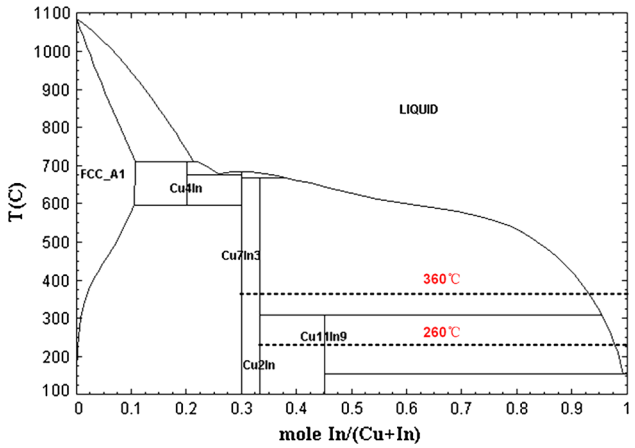


**Fig. 2** Cu–In binary phase diagram

have studied phase transformation mechanisms of Ag–Sn and Ag–In interconnections. They found that $Ag_3Sn$ firstly generated in Ag–Sn interconnections bonded at 320 °C for 8 h. The phase transformation process from $Ag_3Sn$ to $Ag_5Sn$ was accomplished when bonding time reached to 60 min. For Ag–In interconnections bonded at 320 °C for 280 min, $Ag_9In_4$ firstly generated and transformed to $Ag_3In$ in 30 min. Sommadoosi [20] has found that Cu and In could react in different ways at different temperatures. $Cu_{11}In_9$ firstly generates when the bonding temperature is below 310 °C while $Cu_2In$ could generate firstly with higher temperature.

Lin et al. [8] have studied shear properties of Ag–In interconnections. It was found that the solder joints with 3 μm-in-thickness had better shear strengths compared with solder joints with 8 μm-in-thickness. The results also showed that the smaller joints mainly consisted of $Ag_2In$ while the bigger one consisted of $AgIn_2$, which indicated that $AgIn_2$ could decrease the shear properties of solder joints.

Huebner et al. [21] have proved that solder joints formed through SLID method had excellent reliability by thermal cycling tests. Cao et al. [22] have performed the vacuum sealing process of MEMS components through Cu–Sn SLID bonding process under 350 °C peak temperature with 10 min. The formed solder seam which was consisted of $Cu_6Sn_5$ and $Cu_3Sn$ had the shear strength of 19.5 Mpa with excellent sealing performance.

In the paper, Cu/In/Cu joints were prepared under different bonding parameters to analyze phase transformation process of Cu–In intermetallic compounds. Shear tests were conducted to examine the shear strength of Cu/In/Cu joints. Fracture behaviors of different Cu–In joints were also analyzed through fractography.

## 2 Experimental materials and methods

The designed structure of Cu/In/Cu joints was shown in Fig. 1. The size of Si substrate is 1 cm × 1 cm × 0.1 cm. The Ti adhesive layer and Cu seed layer were magnetron sputtered firstly on Si substrate and their thicknesses were 100 nm and 1 μm, respectively. Then 10 μm Cu layer and 6 μm In layer were electroplated onto Cu seed layer. Finally, the metal layers were annealed in air atmosphere at 300 °C for 1 h with heating rate of 5 °C/min.

According to Cu–In binary phase diagram shown in Fig. 2, Cu–In intermetallic compounds evolution process differs at 307 °C. Therefore, 360 and 260 °C were selected as bonding temperatures to study different phase transformation processes in Cu/In/Cu joints in our experiments.

The joints used in shearing tests were bonded at two different temperature (260 and 360 °C) with different times (40, 160 and 360 min, respectively). Three samples were prepared under each bonding condition. The device applied for shear tests was 5948 Micro-Tester produced by Instron Company. The maximum tensile force which can be applied was 500 N. The applied shear speed was 300 μm/min. The shear test will be terminated when the tensile force decreased by 40 % or the tensile force reach up to 480 N. Fracture behavior was then analyzed with Quanta 200F FEI Scanning Electron Microscopy (SEM) and the

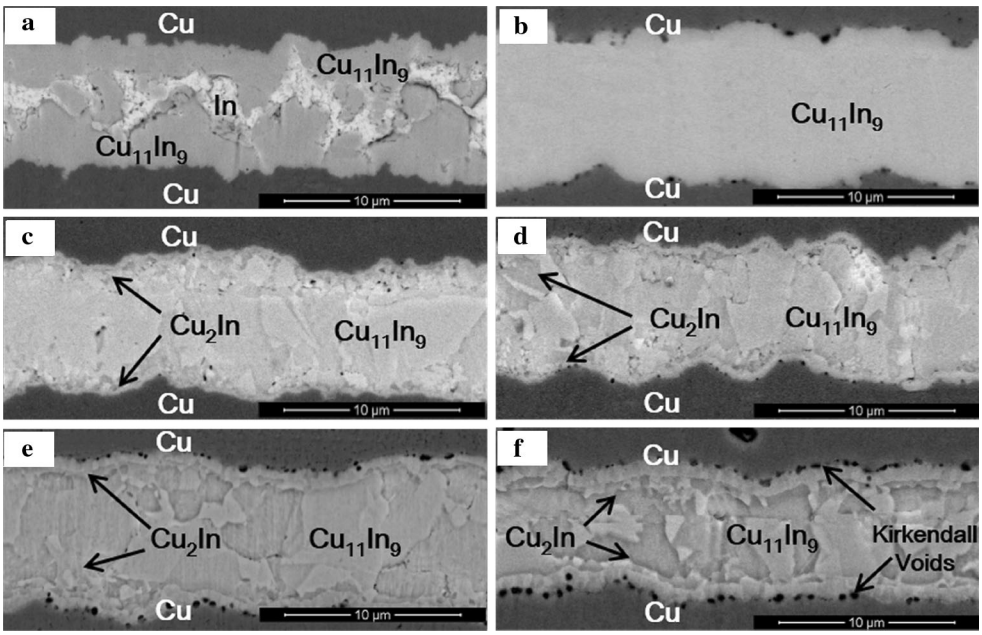


**Fig. 3** Cross-sectional SEM of solder joints bonding at 260 °C for different times. **a** 10 min, **b** 40 min, **c** 160 min, **d** 250 min, **e** 360 min, **f** 810 min

IMC phases were identified by D/max-rB X-ray Detector (XRD).

## 3 Results and discussion

### 3.1 Phase transformation

#### *3.1.1 Microstructure evolution of Cu/In/Cu joints bonded at 260 °C*

The cross-sectional SEM images of Cu/In/Cu joints bonded at 260 °C for different times were shown in Fig. 3.

Figure 3a shows that Cu/In/Cu joints bonded for 10 min mainly consisted of Cu and In intermetallic compounds growing unevenly along Cu substrate surface, which was identified by EDX as $Cu_{11}In_9$. The residual In was isolated as the island shape by the new formed $Cu_{11}In_9$ grains in the middle of the joint. As the bonding time prolonged, In was gradually consumed to react with Cu. When the bonding time reached to 40 min, In was completely consumed and the joint was entirely composed by $Cu_{11}In_9$, as shown in Fig. 3b. In the joints bonded after 160 min, a thin layer of $Cu_2In$ (identified by EDX) formed at the interface between Cu layer and $Cu_{11}In_9$ layer. The thickness of the $Cu_2In$ layer was less than 1 μm. When the bonding times were 250 min and 360 min, the microstructures in Cu/In/Cu joints were similar, as shown in Fig. 3d, e. The $Cu_{11}In_9$ phase was in the middle of the joint and the $Cu_2In$ phase was between the Cu layer and $Cu_{11}In_9$ layer. The $Cu_2In$ layer grew up to 1 μm in thickness. With longer bonding time, the $Cu_2In$ layer grew up to 2 μm in thickness, as shown in Fig. 3f, which indicated that the growth rate of $Cu_2In$ was very low at 260 °C.

It was clear that Kirkendall effect was significant during the microstructure evolution in Cu/In/Cu joints. After the joints were bonded for 40 min, Kirkendall voids occurred along the Cu layer, as was shown in Fig. 3b. With longer reaction times, more $Cu_2In$ was produced and the Kirkendall effect became more serious, as was shown in Fig. 3f, which was the result of phase transformation process between different Cu–In intermetallic compounds. Figure 4 shows the microstructure evolution of Cu/In/Cu joints formed at 260 °C.

#### *3.1.2 Microstructure evolution of solder joints bonding at 360 °C*

The microstructures of Cu/In/Cu joints bonded at 360 °C for different times was shown in Fig. 5. The IMC phase in Cu/In/Cu joints bonded for 10 min was mainly $Cu_2In$, as shown in Fig. 5a. The residual In exhibited the islanded shape. When the bonding time reached to 40 min, the joint was only composed by $Cu_2In$, as shown in Fig. 5b. According to Cu–In phase diagram, the phase transformation from $Cu_2In$ to $Cu_7In_3$ would happen when the temperature was more than 307 °C. As In was completely consumed after 40 min, the $Cu_2In$ would continue to react with Cu elements from the Cu layer. Hence, an obvious IMC layer was found at the interface of solder and Cu

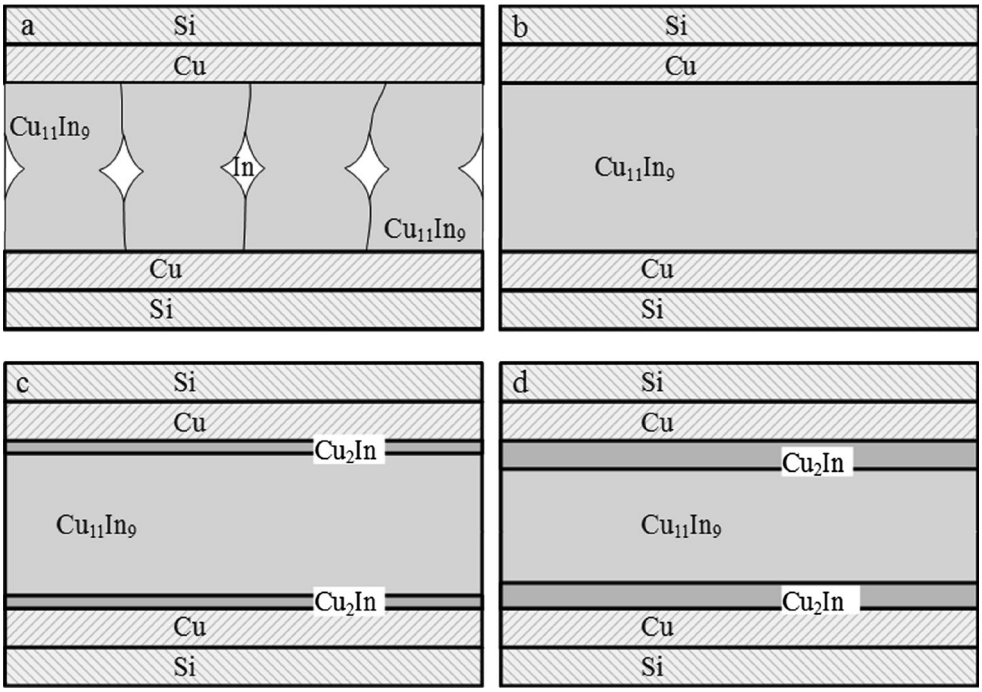


**Fig. 4** Schematic drawing of microstructure evolution of Cu/In/Cu joints formed at 260 °C. **a** Formation of $Cu_{11}In_9$ and isolated In islands, **b** formation of $Cu_{11}In_9$ joint, **c** nucleation of $Cu_2In$ phase, **d** Growth of $Cu_2In$ phase

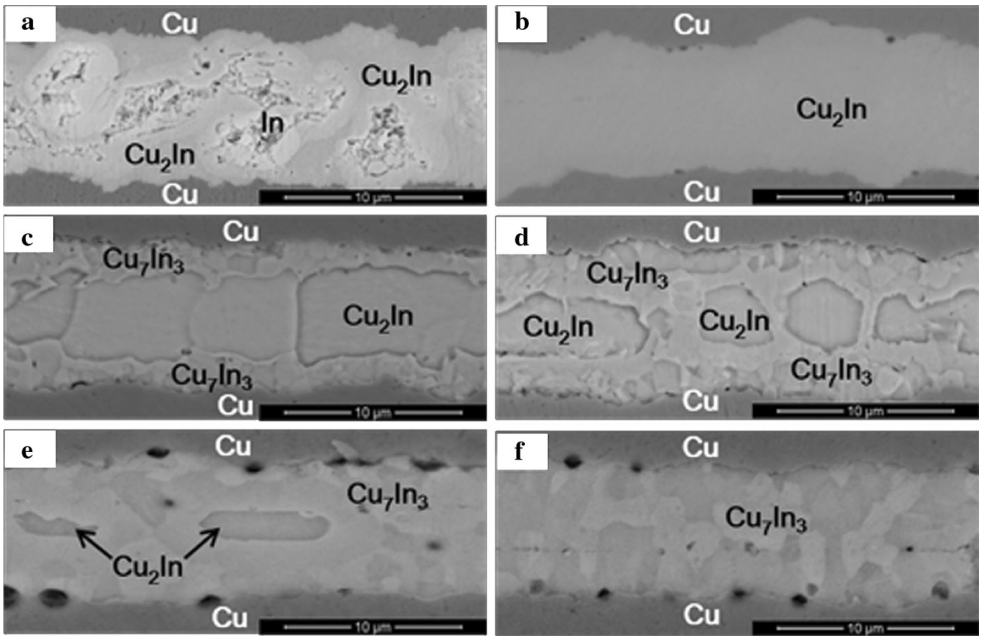


**Fig. 5** Cross-sectional SEM images of solder joints bonded at 360 °C for different times. **a** 10 min, **b** 40 min, **c** 90 min, **d** 160 min, **e** 250 min and **f** 360 min

layer, as shown in Fig. 5c. The layer was confirmed as the $Cu_7In_3$ by EDX. $Cu_7In_3$ grains would keep growing up with the bonding time. At this moment, the $Cu_2In$ phase exhibited the island-shape which was similar to the isolated In shown in Fig. 5a, as was shown in Fig. 5e. When the bonding time reached 360 min, the phase transformation process from $Cu_2In$ to $Cu_7In_3$ was completely finished and the fully $Cu_7In_3$ joint were formed, as was shown in Fig. 5f.

During the phase transformation process from $Cu_2In$ to $Cu_7In_3$, it was also found that $Cu_7In_3$ grains did not grow with a uniform rate but with a higher growth rate along $Cu_2In$ grain boundaries. This was attributed to the diffusion rate of Cu atoms along the grain boundaries of $Cu_2In$ was

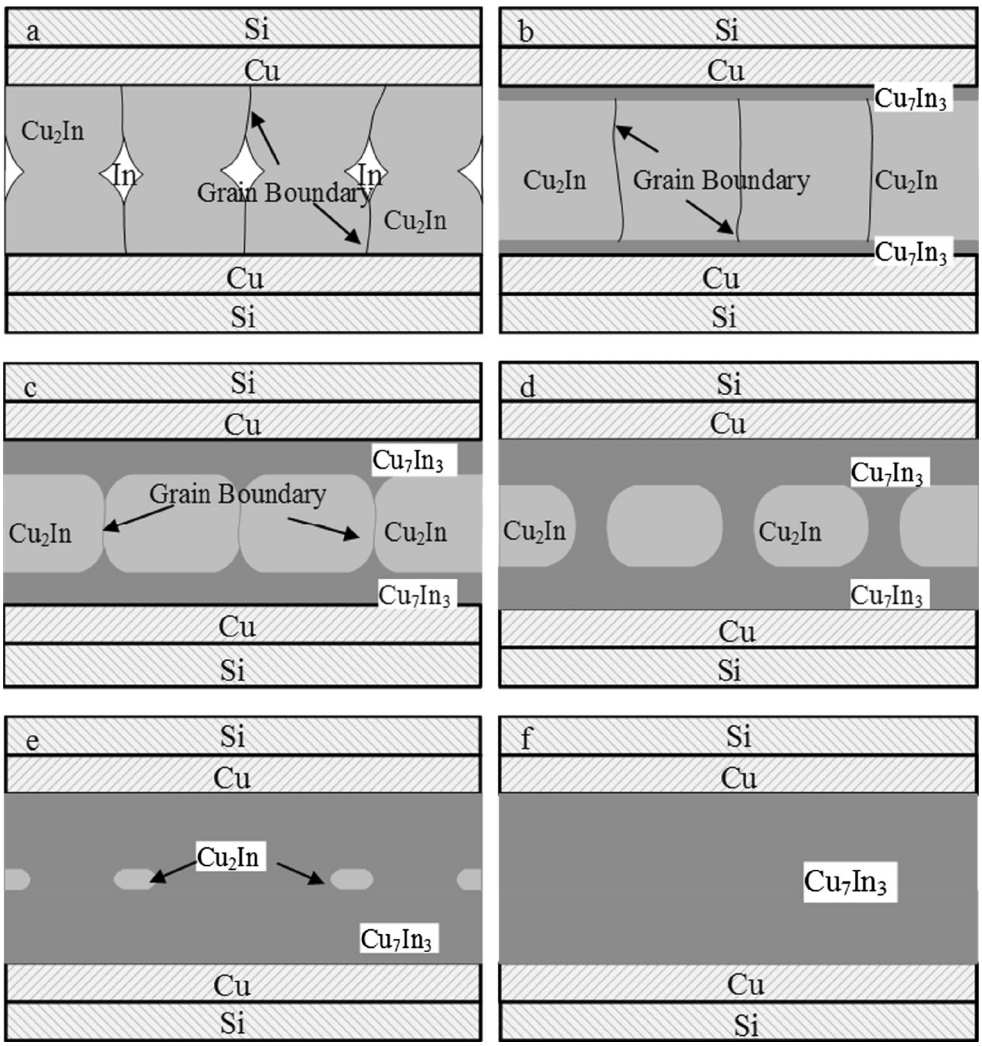


**Fig. 6** Schematic drawing of microstructure evolution of Cu/In/Cu joints formed at 360 °C. **a** Formation of $Cu_2In$ and isolated In islands, **b** formation of $Cu_2In$ joint, **c** preferred nucleation of $Cu_7In_3$ along the grain boundaries of phase $Cu_2In$, **d** growth of $Cu_7In_3$ phase, **e** $Cu_2In$ phases were almost consumed, **f** fully $Cu_7In_3$ joint

higher than that of inside the $Cu_2In$ grains, so that the $Cu_7In_3$ phase preferred grew along the grain boundaries of $Cu_2In$ phase. This process can be explained by the theory of grain boundary coverage transition proposed by Straumal et al. They observed the GB wetting transition can processed not only by the liquid phase in Cu–In system [23] but also by the second solid phase in Al–Mg and Cu–Co system [24, 25]. In this paper, with the Cu atoms diffused in the In matrix continuously, the Cu content in the solder increased, and then the amount of $Cu_7In_3$ phase increased too. When the bonding time was up to 90 min, as seen in Fig. 5c, the coverage of $Cu_2In/Cu_2In$ grain boundaries by the second solid phase $Cu_7In_3$ was incomplete. However, during the bonding time from 90 to 250 min, as shown in Fig. 5c–e, the transition from incomplete to complete coverage of $Cu_2In/Cu_2In$ grain boundaries by $Cu_7In_3$ phases was observed. The complete coverage can be proved by the criterion from the Cahn's work: "if the minor phase wets GBs, the major phase is distributed as droplets in the minor phase" [26]. The major phases (Cu2In) were distributed as island-shape in the minor phases (Cu7In3), as seen in the Fig. 5d–e. Lastly, with both the Cu atoms diffusion and coverage process continuing, the fully Cu7In3 joint were formed, as was shown in Fig. 5f. Based on the above analysis, the microstructure evolution model of Cu/In/Cu joints formed at 360 °C was shown in Fig. 6.

It can be inferred according to Cu–In diagram that phase transition process in Cu/In/Cu joints bonded at 260 °C could be formulated as Eqs. (1) and (2). For joints bonded at 360 °C, the process could be formulated as Eqs. (3) and (4). The different reaction mechanisms under different reaction temperatures brought the different phase transformation processes in Cu/In/Cu interconnections system.

$$11Cu + 9In \rightarrow Cu_{11}In_9 \quad (1)$$

$$Cu_{11}In_9 + 7Cu \rightarrow 9Cu_2In \quad (2)$$

$$2Cu + In \rightarrow Cu_2In \quad (3)$$

$$3Cu_2In + Cu \rightarrow Cu_7In_3 \quad (4)$$

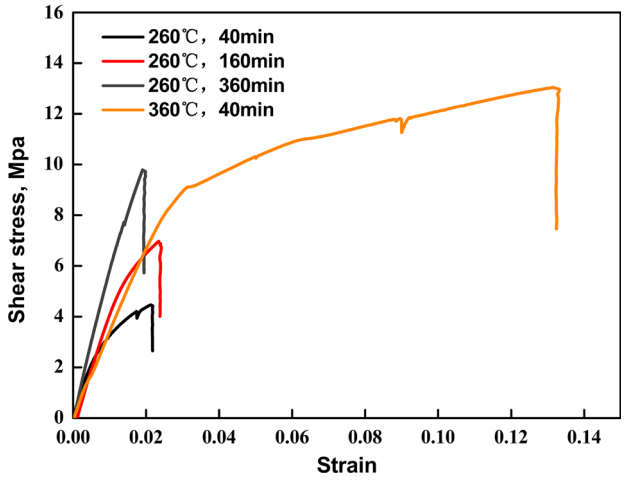


**Fig. 7** Stress–strain curves of solder joints bonded at different temperatures for different times

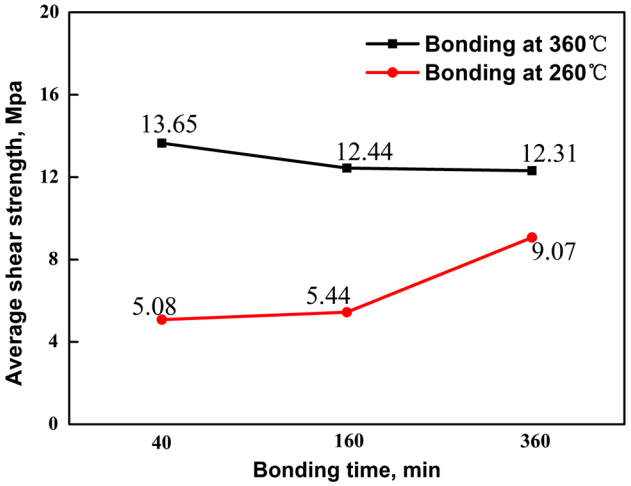


**Fig. 8** Average shear strengths of solder joints bonding for 40, 160 and 360 min

In addition, when the Cu/In/Cu solder joints bonded at 360 °C, the phases were transformed from incomplete to complete coverage of $Cu_2In/Cu_2In$ grain boundaries by $Cu_7In_3$ phases obviously. Compared with that case, there was no $Cu_{11}In_9/Cu_{11}In_9$ grain boundaries wetted or covered by the second solid phases $Cu_2In$ at 260 °C. In other words, the $Cu_{11}In_9/Cu_{11}In_9$ grain boundaries were "dry". We propose that there is a temperature threshold of grain boundaries wetted by the solid phase in Cu–In system in alloy phase diagram. Below this temperature threshold, no $Cu_{11}In_9/Cu_{11}In_9$ grain boundaries are wetted by the solid phases $Cu_2In$. The bonding temperature, 260 °C, may just below this temperature threshold, which is the reason for the "dry" $Cu_{11}In_9/Cu_{11}In_9$ grain boundaries.

## 3.2 Shear strength of Cu/In/Cu interconnections

Stress–strain curves of solder joints bonded under different parameters were measured by shear tests, as was shown in Fig. 7. The results showed that the fracture mode of all samples was brittle fracture. The pre-broken process was partially found in samples, indicating that joints firstly fractured in locations where cracks initiated easily, while other locations of Cu/In/Cu joints were not affected until solder joints was totally fractured. From Fig. 7, it can be found that the joints formed at 360 °C for 40 min has better ductility before fracture, which was attributed to the good ductility of $Cu_2In$ phase inside the joints.

As shown in Fig. 8, the average shear strengths of Cu/In/Cu joints bonded at 260 °C for 40, 160 and 360 min were 5.08, 5.44 and 9.07 Mpa respectively. It was indicated that shear strengths of joints were improved as the bonding time prolonged, specially significantly improved in the joints bonded with 360 min. According to microstructure evolution process, the phase transformation from $Cu_{11}In_9$ to $Cu_2In$ happened in Cu/In/Cu joints bonded at 260 °C, indicating that the $Cu_2In$ phase had better shear property compared to $Cu_{11}In_9$ phase. As the melting point of $Cu_2In$ was much higher than that of $Cu_{11}In_9$, the $Cu_2In$ phase was more stable thermally and more suitable to improve the mechanical properties of Cu/In/Cu interconnections.

Average shear strengths of Cu/In/Cu joints bonded at 360 °C for 40, 160 and 360 min were 13.65, 12.44 and 12.31 Mpa respectively. The shear strength values were higher than that of Cu/In/Cu joints bonded at 260 °C. According to Cu–In phase diagram, the IMC phase has transformed from $Cu_2In$ to $Cu_7In_3$, which would decrease shear strengths of Cu/In/Cu joints. The analysis proved that the shear property of $Cu_7In_3$ was worse than that of $Cu_2In$. As melting points of two phases were almost the same, it was not necessary to obtain $Cu_7In_3$ phase by long-time heating process, instead, relatively good mechanical properties could be achieved by short-time heating process to obtaining solder joints consisted of $Cu_2In$ through short-time heating process.

## 3.3 Fracture behavior of Cu/In/Cu joints

### *3.3.1 Fracture of Cu/In/Cu joints bonded at 260 °C*

Morphology of shear fracture in Cu/In/Cu joints bonded at 260 °C was shown in Fig. 9.

For joints bonded for 40 min, the shear surface was relatively uniform and flat, as shown in Fig. 9a. The fracture mode was mainly cleavage fracture. The content of In

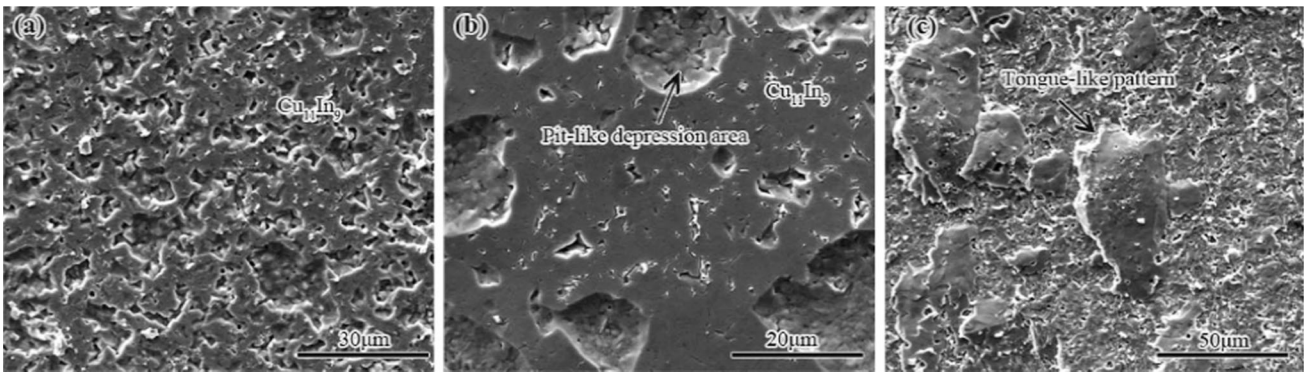


**Fig. 9** Morphology of Shear fracture in Cu/In/Cu joints bonded at 260 °C for different times. **a** 40 min, **b** 160 min, **c** 360 min

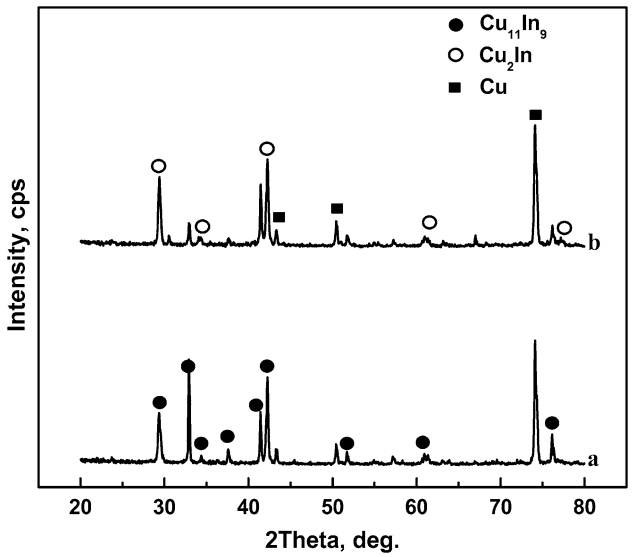


**Fig. 10** XRD spectrums of fractures in Cu/In/Cu joints bonded at 260 °C for different times. **a** 40 min, **b** 360 min

element at the fracture location was 42.96 %, which was confirmed by EDX. It was indicated that the fracture occurred in the $Cu_{11}In_9$ layer. The fracture in Cu/In/Cu joints bonded at 260 °C for 160 min was shown in Fig. 9b. It mainly contained two kinds of morphologies, one was relatively flat and another was the pit-like depression areas. The fracture mode of flat areas was cleavage fracture at the $Cu_{11}In_9$ layer. The pit-like depression areas consisted of $Cu_{11}In_9$ free-growing grains (both identified by EDX). As the roughness of In layers was quite high, gas could hardly get out of joints and as a consequence the voids were formed during solder solidification process. Besides, voids were also the result of agglomeration process of In atoms. The formation of voids in the joints provided the growth conditions for these free-growing $Cu_{11}In_9$ grains. The fracture in Cu/In/Cu joints bonded at 260 °C for 360 min was shown in Fig. 9c. Tongue-like patterns which was the characteristic of cleavage fracture and quasi-cleavage fracture were found at fracture location. During crack propagation, secondary cleavage and local tearing phenomenon of metals happened along planes between main cleavage planes and twin planes. The existence of tongue-like patterns indicated that plasticity and toughness of the Cu/In/Cu joints were improved. According to analysis of microstructure and data of shear strength, it was proved that $Cu_2In$ has better plasticity and toughness, than $Cu_{11}In_9$.

XRD test was conducted to determine the IMC phases at the fracture locations, as shown in Fig. 10. Comparing XRD spectrums of fractures in Cu/In/Cu joints bonded at 260 °C, it was found that intensity of $Cu_{11}In_9$ diffraction peak decreased while that of $Cu_2In$ increased as the bonding time. The result confirmed the phase transformation process from $Cu_{11}In_9$ to $Cu_2In$. It was also found that the intensity of $Cu_{11}In_9$ diffraction peak was relatively high at the fracture locations in Cu/In/Cu joints bonded for 360 min, which indicating that joints only composed by $Cu_2In$ could be obtained through relatively longer bonding time.

### *3.3.2 Fracture of Cu/In/Cu joints bonded at 360 °C*

Morphology of shear fracture in Cu/In/Cu joints bonded at 360 °C was shown in Fig. 11. River-like patterns and cleavage steps were found at the fracture location of Cu/In/Cu joints, indicating that the fracture mode was cleavage fracture. Tongue-like patterns were also found at fracture location in Cu/In/Cu joints bonded for 40 and 160 min, as shown in Fig. 11a, b. The tongue-like patterns indicated that Cu/In/Cu joints showed the plastic toughness. The IMC phases on the fracture locations were determined to be $Cu_2In$ using EDX. For Cu/In/Cu joints bonded for 360 min, as shown in Fig. 11c, the content of In element at fracture location was 29.97 %, which indicating that the fracture was located between $Cu_7In_3$ layer and $Cu_2In$ layer. In addition to the river-like patterns and cleavage stages. The smooth grain surface indicated that the fracture mode was

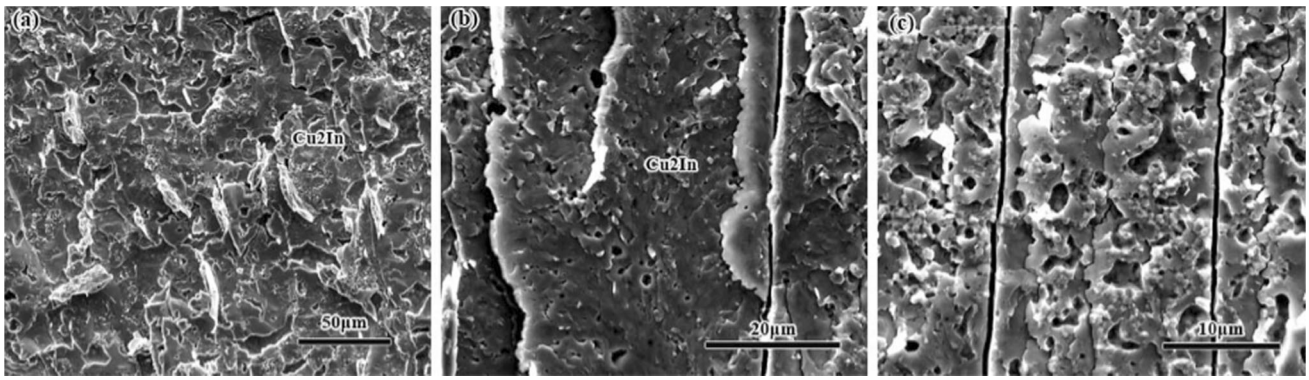


**Fig. 11** Shear fracture morphology of Cu/In/Cu joints bonded at 360 °C for different times. **a** 40 min, **b** 160 min, **c** 360 min

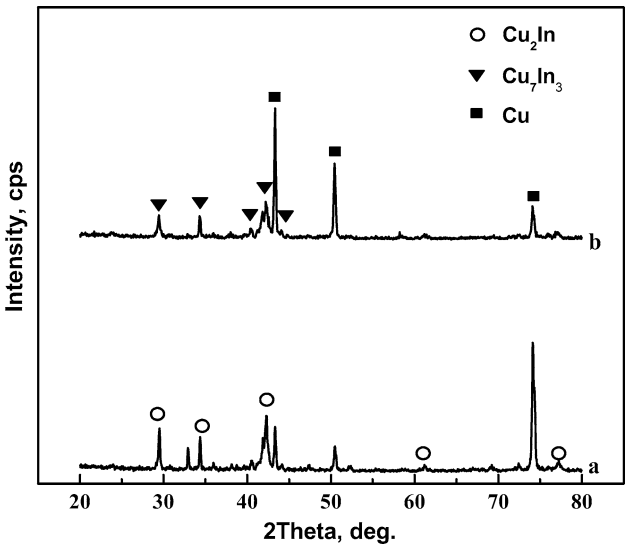


**Fig. 12** XRD spectrum of fracture in Cu/In/Cu joints bonded at 360 °C for different times. **a** 40 min, **b** 360 min

intergranular fracture. According to microstructure analysis, the cleavage fracture was located at the position where the $Cu_7In_3$ phase was formed while the intergranular fracture was located at the interface between $Cu_7In_3$ layer and $Cu_2In$ layer. Stress concentration was generated at the interface due to the phase transformation, the intergranular fracture preferred to occur in these areas.

XRD spectrums of fractures in Cu/In/Cu joints bonded at 360 °C were shown in Fig. 12. It was found that the Cu/In/Cu joints formed at 360 °C for 40 min mainly consisted of $Cu_2In$ and the Cu/In/Cu joints formed at 360 °C for 360 min consisted of $Cu_7In_3$, which was in agreement to the above microstructure analysis.

## 4 Conclusions

In this study, phase transformation and fracture behavior in Cu/In/Cu interconnection formed by SLID bonding was studied. For Cu/In/Cu joints bonded at 260 °C for short time, scallop-shaped $Cu_{11}In_9$ was generated until In elements were consumed completely. $Cu_2In$ was generated on the interface of $Cu_{11}In_9$ and Cu with a quite low nucleation rate. For solder joints bonded at 360 °C, $Cu_2In$ was firstly generated, and then transferred into $Cu_7In_3$ with a relatively high nucleation rate.

According to result of shear test, shear strength of solder joints bonded at 260 °C was increased as bonding time prolonged, especially for those bonded for 360 min, indicating that $Cu_2In$ improved shear property of Cu/In/Cu joints. However, shear strength of solder joints bonded at 360 °C did not change much as bonding time changed, indicating that $Cu_7In_3$ could not improve shear property. $Cu_2In$ was high-quality phase which could improve the mechanical properties of Cu/In/Cu joints.

The fracture mode of solder joints bonded at 260 °C was cleavage fracture, and fracture was located on layers of $Cu_{11}In_9$. Similarly, fracture mode of solder joints bonded at 360 °C for 40 and 160 min was cleavage fracture, and fracture was located on layers of $Cu_2In$, and tongue-like patterns were also found. However, for solder joints bonded for 360 min, fracture mode on the interface of $Cu_2In$ and $Cu_7In_3$ was intergranular fracture, while fracture mode on the layer of $Cu_7In_3$ was cleavage fracture.

**Acknowledgments** The authors are grateful for financial support from the National Science Foundation of China (Grant No. 51075103) and support from Program for New Century Excellent Talents in University (NCET-13-0175).

## References

1. C.-T. Ko, K.-N. Chen, Microelectron. Reliab. **50**, 481 (2010)
2. Y. Cao, W. Ning, L. Luo, IEEE Trans. Electron. Packag. Manuf. **32**, 125 (2009)
3. K. Sakuma, P. Andry, B. Dang, J. Maria, C. Tsang, C. Patel, S. Wright, B. Webb, E. Sprogis, S. Kang, in *Proceeding of 57th Electronic Components and Technology Conference* (2007), p. 627

4. A. Klumpp, R. Merkel, R. Wieland, P. Ramm, in *Electronic Components and Technology Conference, 2003. Proceedings. 53rd.* (2003), p. 1080
5. B. Gollas, J.H. Albering, K. Schmut, V. Pointner, R. Herber, J. Etzkorn, Intermetallics **16**, 962 (2008)
6. S. Sommadossi, L. Litynska, P. Zieba, W. Gust, E. Mittemeijer, Mater. Chem. Phys. **81**, 566 (2003)
7. S. Sommadossi, W. Gust, E. Mittemeijer, Mater. Chem. Phys. **77**, 924 (2003)
8. J.-C. Lin, L.-W. Huang, G.-Y. Jang, S.-L. Lee, Thin Solid Films **410**, 212 (2002)
9. H. Liu, G. Salomonsen, K. Wang, K.E. Aasmundtveit, N. Hoivik, IEEE Trans. Compon. Packag. Manuf. Technol. **1**, 1350 (2011)
10. C. Yuhan, L. Le, J. Semicond. **30**, 086001 (2009)
11. T. Takahashi, S. Komatsu, T. Kono, Electrochem. Solid-State Lett. **12**, H263 (2009)
12. N. Bosco, F. Zok, Acta Mater. **52**, 2965 (2004)
13. W.K. Choi, D. Yu, C. Lee, L. Yan, A. Yu, S.W. Yoon, J.H. Lau, M.G. Cho, Y.H. Jo, H.M. Lee, in *58th Electronic Components and Technology Conference* (2008), p. 1294
14. J. Li, P. Agyakwa, C. Johnson, Acta Mater. **58**, 3429 (2010)
15. A. Wronkowska, A. Wronkowski, K. Kukliński, M. Senski, Ł. Skowroński, Appl. Surf. Sci. **256**, 4839 (2010)
16. J. Li, P. Agyakwa, C. Johnson, Acta Mater. **59**, 1198 (2011)
17. G.-T. Lim, B.-J. Kim, K. Lee, J. Kim, Y.-C. Joo, Y.-B. Park, J. Electron. Mater. **38**, 2228 (2009)
18. B. Lee, J. Park, S.-J. Jeon, K.-W. Kwon, H.-J. Lee, J. Electrochem. Soc. **157**, H420 (2010)
19. C. Lee, A. Yu, L. Yan, H. Wang, J.H. He, Q.X. Zhang, J.H. Lau, Sens. Actuators, A **154**, 85 (2009)
20. S. Sommadossi, W. Gust, E. Mittemeijer, Mater. Sci. Technol. **19**, 528 (2003)
21. H. Huebner, S. Penka, B. Barchmann, M. Eigner, W. Gruber, M. Nobis, S. Janka, G. Kristen, M. Schneegans, Microelectron. Eng. **83**, 2155 (2006)
22. Y. Cao, W. Ning, L. Luo, IEEE. Trans. Electron. Pack. **32**, 125 (2009)
23. A. Straumal, B. Bokstein, A. Petelin, B. Straumal, B. Baretzky, A. Rodin, A. Nekrasov, J. Mater. Sci. **47**, 8336 (2012)
24. B. Straumal, O. Kogtenkova, A. Straumal, Y.O. Kuchyeyev, B. Baretzky, J. Mater. Sci. **45**, 4271 (2010)
25. B. Straumal, B. Baretzky, O. Kogtenkova, A. Straumal, A. Sidorenko, J. Mater. Sci. **45**, 2057 (2010)
26. J.W. Cahn, Phys. A **279**, 195 (2000)